tvst

Lens

Visualization of Cataract Surgery Steps With 4D Microscope-Integrated Swept-Source Optical Coherence Tomography in Ex Vivo Porcine Eyes

Anja Britten[1], Philipp Matten[2], Jonas Nienhaus[1], Jennifer-Magdalena Masch[3], Katharina Dettelbacher[1], Hessam Roodaki[4], Nancy Hecker-Denschlag[4], Rainer A. Leitgeb[1], Wolfgang Drexler[1], Andreas Pollreisz[5], and Tilman Schmoll[1,6]

[1] Center for Medical Physics and Biomedical Engineering, Medical University of Vienna, Vienna, Austria
[2] Carl Zeiss AG, Eggenstein-Leopoldshafen, Germany
[3] Carl Zeiss Meditec AG, Berlin, Germany
[4] Carl Zeiss Meditec AG, Oberkochen, Germany
[5] Department of Ophthalmology and Optometry, Medical University of Vienna, Vienna, Austria
[6] Carl Zeiss Meditec, Inc., Dublin, CA, USA

Correspondence: Tilman Schmoll, Medical University of Vienna, Waehringer Guertel 18–20, 4L, Vienna, Vienna 1090, Austria. e-mail: tilman.schmoll@zeiss.com

Received: December 22, 2023
Accepted: February 19, 2024
Published: April 12, 2024

Keywords: 4D-OCT; SS-OCT; cataract surgery

Citation: Britten A, Matten P, Nienhaus J, Masch JM, Dettelbacher K, Roodaki H, Hecker-Denschlag N, Leitgeb RA, Drexler W, Pollreisz A, Schmoll T. Visualization of cataract surgery steps with 4D microscope-integrated swept-source optical coherence tomography in ex vivo porcine eyes. Transl Vis Sci Technol. 2024;13(4):18, https://doi.org/10.1167/tvst.13.4.18

Purpose: To investigate the visualization capabilities of high-speed swept-source optical coherence tomography (SS-OCT) in cataract surgery.

Methods: Cataract surgery was simulated in wet labs with ex vivo porcine eyes. Each phase of the surgery was visualized with a novel surgical microscope-integrated SS-OCT with a variable imaging speed of over 1 million A-scans per second. It was designed to provide four-dimensional (4D) live-volumetric videos, live B-scans, and volume capture scans.

Results: Four-dimensional videos, B-scans, and volume capture scans of corneal incision, ophthalmic viscosurgical device injection, capsulorrhexis, phacoemulsification, intraocular lens (IOL) injection, and position of unfolded IOL in the capsular bag were recorded. The flexibility of the SS-OCT system allowed us to tailor the scanning parameters to meet the specific demands of dynamic surgical steps and static pauses. The entire length of the eye was recorded in a single scan, and unfolding of the IOL was visualized dynamically.

Conclusions: The presented novel visualization method for fast ophthalmic surgical microscope-integrated intraoperative OCT imaging in cataract surgery allowed the visualization of all major steps of the procedure by achieving large imaging depths covering the entire eye and high acquisition speeds enabling live volumetric 4D-OCT imaging. This promising technology may become an integral part of routine and advanced robotic-assisted cataract surgery in the future.

Translational Relevance: We demonstrate the visualization capabilities of a cutting edge swept-source OCT system integrated into an ophthalmic surgical microscope during cataract surgery.

Introduction

Optical coherence tomography (OCT) is a valuable tool for preoperative and postoperative examinations in cataract surgery, but it is rarely used intraoperatively, despite the availability of dedicated solutions.[1,2] Preoperative examinations include intraocular lens (IOL) power calculations that are commonly performed using optical biometry devices with an underlying technology similar to OCT.[3] In addition, preoperative OCT imaging of the macula allows the detection of abnormalities that may limit postoperative visual acuity gains.[4] Postoperative OCT imaging focuses on corneal wound[5] and IOL position monitoring,[6] as well as assessment for macular edema.[7]

translational vision science & technology

Intraoperative spectral domain OCT (SD-OCT) has found its way into routine vitreoretinal surgery as it requires less imaging depth than visualizations in anterior segment surgery.[8] SD-OCT is also used for corneal graft procedures, including deep anterior lamellar keratoplasty (DALK), descement stripping automated endothelial keratoplasty (DSAEK), and descemet membrane endothelial keratosplasty (DMEK). The benefits of intraoperative OCT for DMEK have been outlined.[9] Nevertheless, the clinical advantage of diagnostic 1060-nm swept-source OCT (SS-OCT) over 840-nm SD-OCT is well described in the literature. SS-OCT has shown tremendous progress in signal quality, imaging depth, imaging speed, sensitivity, and field of view (FOV).[10] Although intraoperative SS-OCT would benefit from the same advantages, it has not yet been implemented in commercial devices. Nevertheless, intraoperative SS-OCT prototypes have previously been used in both porcine eyes and human surgeries but lack flexibility due to fixed sampling rates, low imaging speed, and small imaging depth.[11–14]

Scenarios in cataract surgery where patients may benefit from intraoperative SS-OCT imaging include the intraoperative calculation of IOL power,[15] which has been shown to result in a more precise lens estimation for patients with prior myopic refractive surgery,[16] or real-time monitoring of lens fragments, which may cause damage to the corneal endothelium.[17] Furthermore, determining the lens position at the end of surgery[18,19] and correcting a displacement or estimating distances for femtosecond laser assisted cataract surgery[20] are of interest.

Carrasco-Zevallos et al.[21] connected a SS-OCT engine to a surgical microscope. This setup served as a visualization platform that not only provides two-dimensional but rather live volumetric images. By using a configurable swept-source laser with variable system parameters capable of adjusting the A-scan rates between 100 kHz and 1.2 MHz, distinct imaging modes can be generated to address a multitude of imaging applications within one engine.[22]

In this article, we present OCT visualizations of all major steps of cataract surgery that were simulated in ex vivo porcine eyes, as well as discuss the enhancement of intraoperative visualizations imaged with a state-of-the-art configurable SS-OCT engine and potential clinical benefits. We provide four-dimensional (4D) videos, as well as volume captures and B-scans.

Methods

We have previously described a novel SS-OCT engine integrated into a surgical microscope (ARTEVO 800; Carl Zeiss Meditec AG, Jena, Germany).[22] This prototype offers various imaging capabilities for different imaging scenarios, such as B-scan crosses, raster capture scans, and live volumetric OCT. The platform can either serve as a real-time visualization tool, where two-dimensional (2D) or three-dimensional (3D) rendered data are displayed stereoscopically in real time, or as a documentation and diagnostic tool to save data for offline analysis. A micro-electromechanical system vertical-cavity surface-emitting laser (MEMS-VCSEL) light source provides the flexibility of toggling between three different laser sweep repetition rates and hence realizing various application-specific imaging modes. For this experimental study, we defined four scan protocols that are based on two laser sweep repetition rates. B-scan crosses and raster capture volumes over a scanned area of 12.7 × 12.7 mm were acquired at 100 kHz and stand out by capturing 29.7 mm in depth at an axial resolution of 6.6 µm in tissue. For 4D volumetric imaging, we increased the sweep repetition rate of the laser to 600 kHz and used a spectral splitting technique[23] to realize an effective A-scan rate of 1.2 MHz. Thereby, we were able to achieve FOVs of 4.5 mm and 9.7 mm in diameter that we scanned in a spiral-shaped fashion at a 10-Hz and 3-Hz volume rate, respectively. To achieve a useful FOV for the 4D imaging modes by the abovementioned spectral splitting approach, axial resolution was reduced to 21.6 µm in tissue. The Table summarizes the specifications of the imaging modes used in this study. Switching between imaging modes requires only software changes and can be performed within a couple of seconds.

A trained ophthalmic surgeon (A.P.) performed simulated cataract surgeries in five ex vivo porcine eyes, which were obtained from a local butcher (Fleischerei Hödl, Vienna, Austria). While porcine animal models are commonly employed to mimic the human eye, they do not fully replicate the conditions found in humans.[24] In addition, the porcine eyes used in this study originated from juvenile swine, resulting in soft corneas and soft lenses without cataracts, which are not representative of the use case for human eyes. Nevertheless, they allowed for a first evaluation of the technical application.

The surgical steps included in our simulated cataract surgeries are clear corneal incision, ophthalmic viscosurgical device (OVD) injection, capsulorrhexis, phacoemulsification, and IOL injection. The following ophthalmic surgical equipment was utilized: 2.4-mm slit-angled ophthalmic knife (MSL24; Mani, Inc., Utsunomiya, Japan), capsulorrhexis forceps (2-716G-8R; Duckworth & Kent LTD, Baldock, United Kingdom), OVD (Z-Hyalin; Carl Zeiss Meditec AG) injected with a 27-gauge cannula (Viscoflow Cannula;

Table. Technical Specifications of Imaging Modes

Pattern	4D-OCT 1	4D-OCT 2	B-scan Line	Raster Capture
Effective A-scan rate	1.2 MHz	1.2 MHz	100 kHz	100 kHz
FOV	4.5 mm (spiral diameter)	9.7 mm (spiral diameter)	12.4 mm (line width)	12.4 mm (square diameter)
Imaging depth	5.1 mm	5.1 mm	29.7 mm	29.7 mm
Volume rate	10 Hz	3 Hz	NA	NA
Axial resolution	21.6 µm in tissue	21.6 µm in tissue	6.6 µm in tissue	6.6 µm in tissue

NA, not applicable.

Beaver-Visitec International, Inc., Waltham, MA, USA), phacoemulsification system (Zeiss Visalis V500; Carl Zeiss Meditec AG) with a 22-gauge phacoemulsification set (phaco set plus 22 gauge, biconical 30°; Carl Zeiss Meditec AG), and intraocular lens (CT Asphina 409MP; Carl Zeiss Meditec AG) injected with an injector set (Bluemixs 180; Carl Zeiss Meditec SAS). The surgeon was able to view the 4D-OCT images during the mock surgery on the 3D screen but relied only on the conventional microscopic visualization through the oculars to perform the procedures. An assistant operated the OCT engine and acquired OCT data in parallel. We recorded videos of the surgical steps and saved additionally raw data for offline reconstruction of the entire length of the eye at the end of the surgery. To visualize the unfolding process of the IOL and its position in the capsular bag after unfolding, we processed the data offline with an artificial intelligence-based denoising approach.[25] Even though all data are visualized live, these optional offline processing steps allow us to generated data sets with enhanced image quality.

Results

OCT images of major steps in cataract surgery were successfully obtained. In Figures 1A–D, four frames of a clear corneal incision that were selected from a 4D video are shown. The videos were recorded with the scan pattern 4D-OCT 1 as described in the Table. The volumetric rendering is presented alongside two cross-sectional B-scans and an enface projection. Depth is colorized from red to blue, with structures closer to the top of the image appearing red.[26] In Figures 1A–C, the penetration of the knife in the cornea can be observed, and Figure 1D shows the final incision. A video of this surgical step is provided in Supplementary Video S1. Figures 1E–H visualize the injection of OVD with a 27-gauge cannula. Progressive filling of the anterior chamber with OVD is documented in Figures 1E–H. Prior to the injection shown in Figure 1E, the anterior chamber was rather flat compared to the image in Figure 1H, showing the end of the injection process. The step of OVD injection is also provided in Supplementary Video S2.

After creating the incision and stabilizing the anterior chamber with viscoelastic, the anterior lens capsule was opened with a continuous curvilinear capsulorrhexis, which was imaged with the scan pattern 4D-OCT 2 (Fig. 2). We chose this scan pattern to gain a larger FOV of 9.7 mm compared to the previous videos. An initial radial cut in the capsule was made (Fig. 2A) to create a small flap (Fig. 2B) that was grasped by the surgeon with a forceps (Figs. 2C, 2D) to carry out the circular rhexis. The deformation of the capsule during the radial cut is visible in A. A video recording of the capsulorrhexis is provided in Supplementary Video S3. Figure 3 shows B-scans of phacoemulsification and IOL unfolding, which we imaged using the B-scan line pattern. The B-scans showing phacoemulsification (Figs. 3A–D) are frames selected from a live screen recording. Following the images, one can appreciate the increasing depth of the trench in the lens sculpted by the phacoemulsification probe. The posterior capsule surface is visible during the procedure. Although all B-scans can be viewed live during the procedure, the B-scans showing IOL unfolding (Figs. 3E–G) were reconstructed and denoised offline to enhance the quality of the IOL images. Supplementary Videos S4 and S5 show phacoemulsification and IOL unfolding, respectively. At the end of the procedure, we imaged the position of the IOL in the capsular bag after unfolding with a raster capture scan. We reconstructed, denoised, and rendered this data set offline. Figure 4 presents three rendered perspectives of the same volume, as well as a B-scan of the position of the IOL in the capsular bag. All images were offline reconstructed and averaged five times. The rendering of the position can also be viewed in

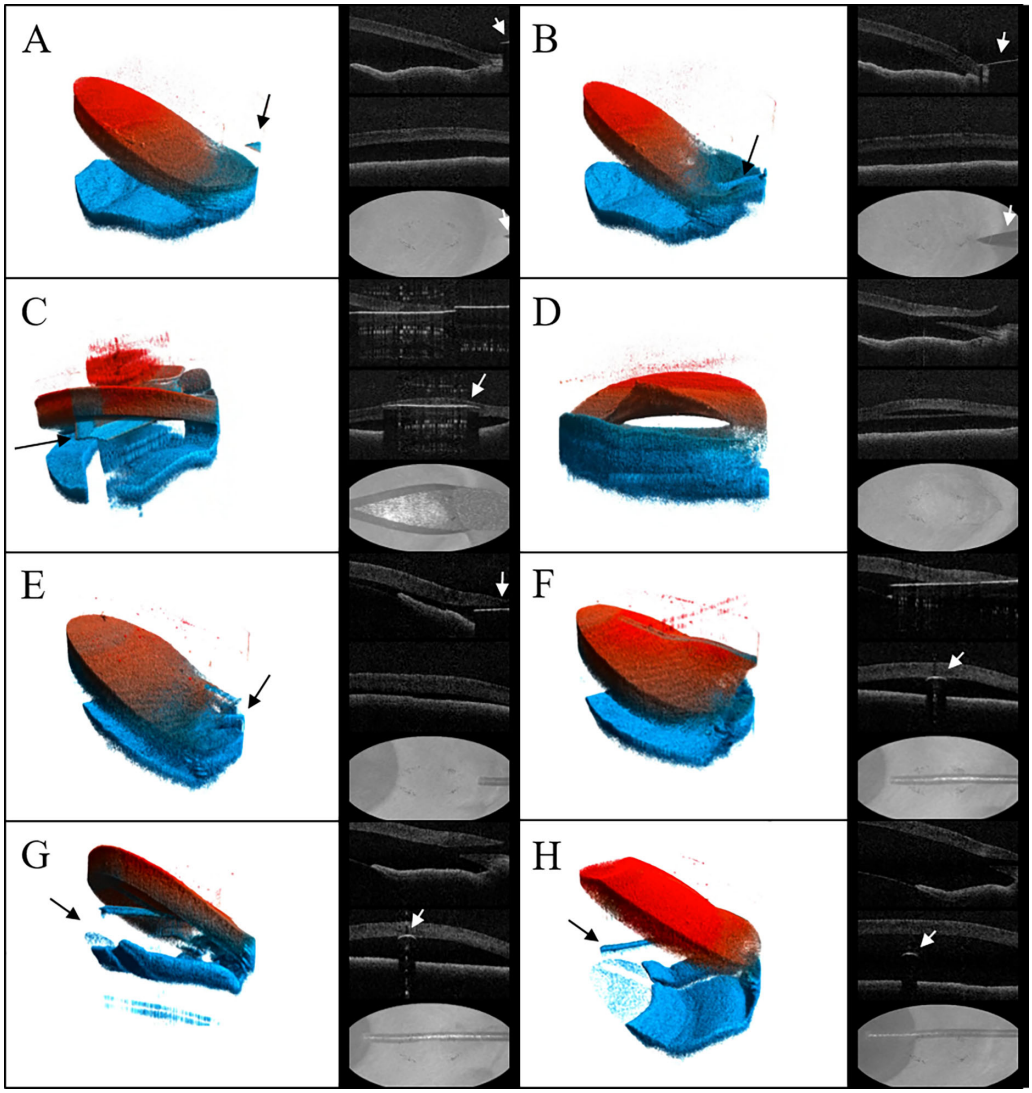

Figure 1. Clear corneal incision (**A–D**) and OVD injection (**E–H**) imaged with 4D-OCT. (**A**) Knife tip above cornea. (**B–D**) Corneal incision. (**E–H**) OVD injection. *Black* and *white arrows* indicate the knife in **A–C**. In **E–H**, *black* and *white arrows* refer to the cannula.

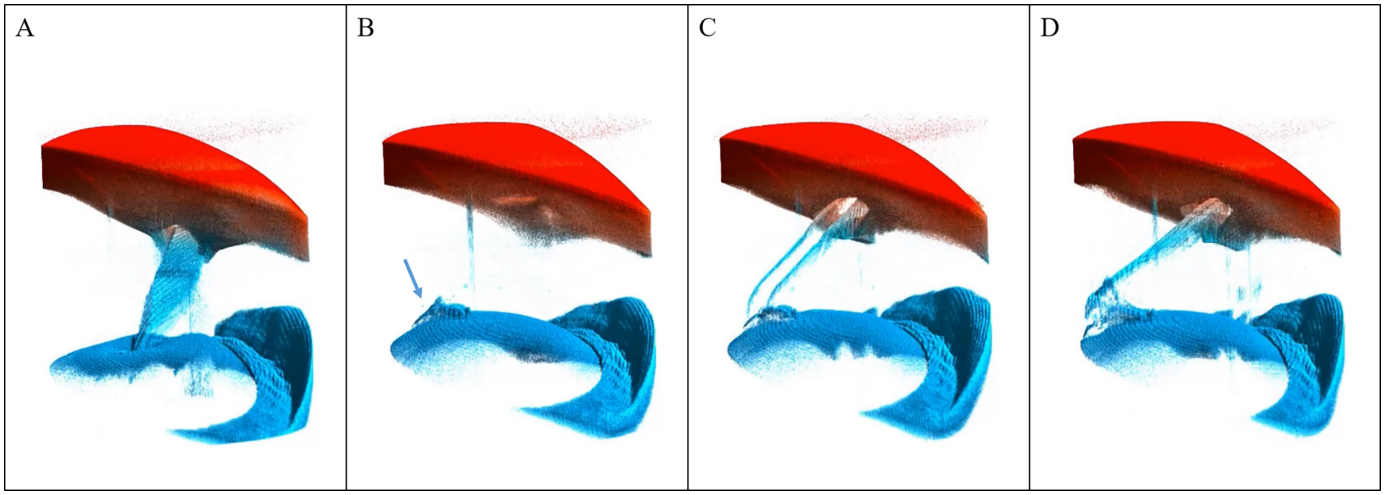

Figure 2. The 4D visualization of capsulorrhexis. (**A**) Initial punctuation of the anterior capsule performed with a slit-angled knife. (**B**) Deformation of initial cut is indicated by the *blue arrow*. (**C**) Forceps inserted through the corneal incision and approaching puncture. (**D**) Forceps grasping initial puncture to create flap.

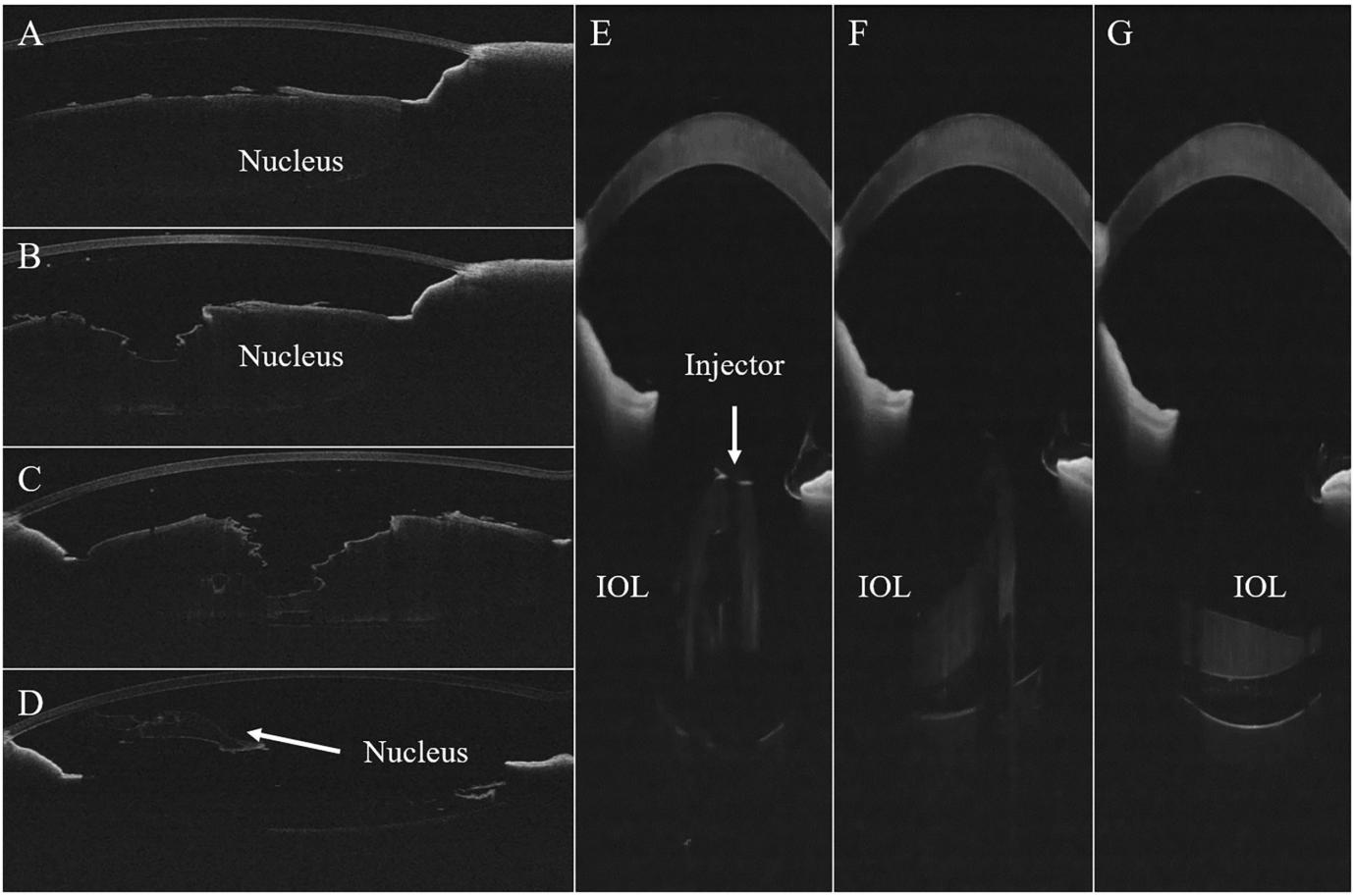

Figure 3. B-scan series of phacoemulsification (**A–D**) and IOL unfolding process (**E–G**). (**A**) Nucleus emulsification has just started. (**B**) A central groove was sculpted in the nucleus with a depth of approximately 50% of the natural lens height. (**C**) The groove was advanced towards posterior. (**D**) The nucleus was removed with a small lens fragment remaining in the anterior chamber. (**E**) IOL is injected in the capsular bag. The IOL unfolding started and the injector is visible. (**F**) IOL unfolding continues. (**G**) Position of IOL in the capsular bag after unfolding.

Supplementary Video S6. To cover a larger FOV, the scanner amplitude was scaled to 1.5, which resulted in a FOV of 18.6 × 18.6 × 29.7 mm. We did not perform lens hydrodissection and corneal incision closing.

Discussion

In this study, we presented novel visualization methods of the fastest ophthalmic surgical microscope-integrated OCT to date. With this setup, we achieved large imaging depth that can cover the entire length of the eye within one acquisition, and its high acquisition speed enabled live volumetric, 4D-OCT imaging. This allowed us to comprehensively visualize four steps of cataract surgery.

Highly scattering structures were effortlessly visualized and displayed with impressive image quality (e.g., the iris). But even the cornea, which only exhibits weak scattering, could be visualized with good contrast. However, IOLs, which are highly transparent even at 1060 nm, only yielded a signal close to the noise floor. But by precisely focusing the OCT beam directly on the IOL, it was possible to obtain their OCT images. Averaging of OCT images allowed for improving the contrast. Moreover, capturing structures larger than our live FOV (e.g., the entire cornea in lateral direction) proved to be difficult and could only be partially recorded live. For an optimal 4D-OCT visualization during cataract surgery, it would certainly be desirable to have a larger FOV and still higher volume rates. Both are, however, limited by the available swept-source lasers and data acquisition systems as well as today's data transfer interfaces and data-processing speeds. To enhance the usability of intraoperative SS-OCT despite its limited FOV, 4D-OCT and surgical microscope image fusion should be investigated.[27] These may

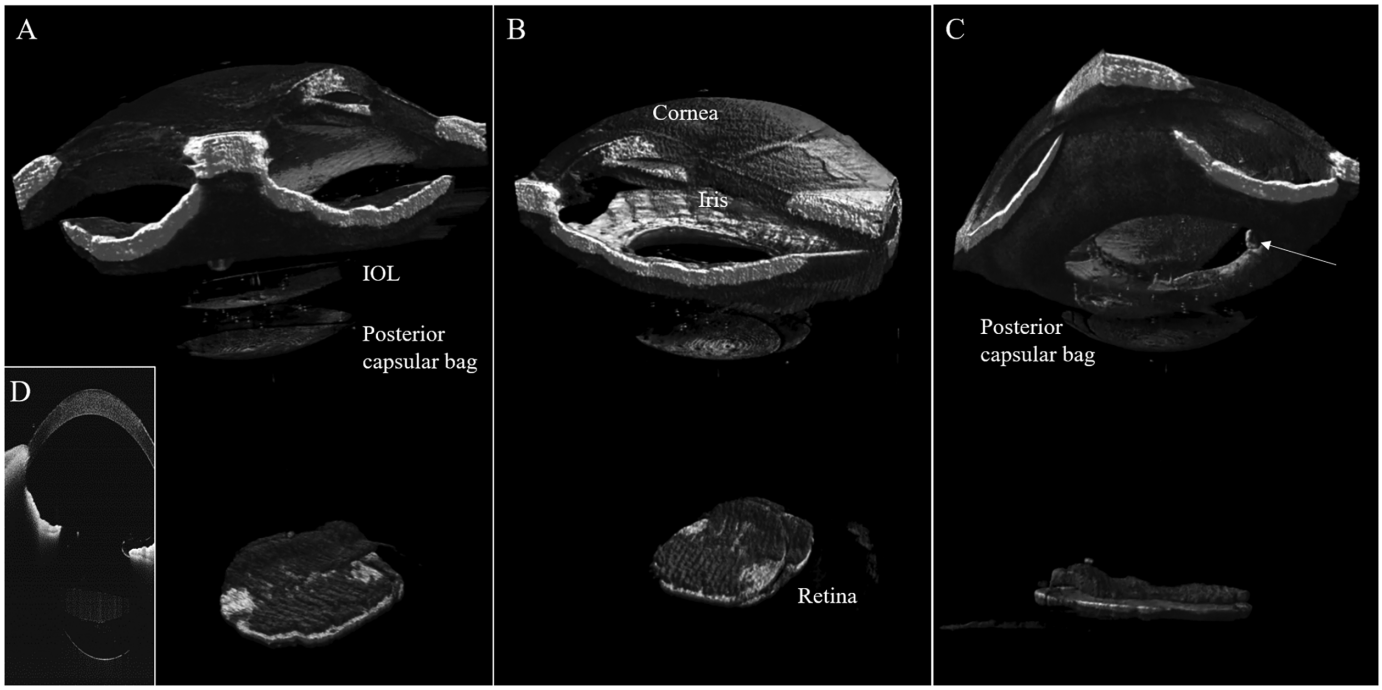

Figure 4. Different perspectives of IOL position in the capsular bag. The entire length of the eye, from cornea to retina, is shown in each scan. Images were averaged five times. (**A**) Rendered raster capture scan demonstrating the IOL position in the capsular bag. (**B**) Iris and capsulorrhexis from the anterior view. (**B**) Capsulorrhexis from the posterior view. The *white arrow* indicates an edge of the flap. (**D**) B-scan of IOL position in the capsular bag. For **A–C**, scanner amplitude is scaled to 1.5 to cover a larger FOV of 18.6 mm.

add specific benefits of 4D-OCT, such as enhanced resolution and depth perception in the relevant center of the FOV or tool tracking at the tip of the instrument, while still retaining the benefits of the traditional surgical microscope view, such as a large FOV for axial and lateral orientation. In addition to better visualization, modern SS-OCT systems offer larger scanning depth with pretty much no signal-to-noise ratio (SNR) loss and a significantly higher data rate. The 4D-OCT devices typically generate several gigabytes of data per second. This exceeds what a human can process by several orders of magnitude, which is why the data stream is eventually presented as a stereoscopic 2D video to the surgeon. Another potential future clinical application is cataract surgery assisted by or even performed autonomously by a surgical robot.[28] Although the visualization and sensing requirements for a robot may differ compared to a human, we believe that robots are much better suited to process the stream of data and may therefore improve outcome and efficiency. A first demonstration of semiautomated lens removal guided by OCT data has already been presented by Chen et al.[29] Intraoperative OCT-guided robotic deep anterior lammelar keratoplasty has also already been reported.[30,31] However, the setups have very limited imaging characteristics regarding their imaging FOVs, flexibility, and their speeds. Heads-up displays enable the simultaneous viewing of the conventional microscope perspective alongside 4D-OCT images. This method of data presentation holds the potential to enhance the current setup, where the surgical maneuvers are limited to the microscopic view through the oculars.

We hypothesize that cataract surgery performed by humans is mainly going to benefit from intraoperative OCT through assistance functions. For instance, OCT can be used to measure the distance between the phacoemulsification tip and the posterior capsular bag in order to issue warnings or reduce ultrasound power as the surgeon approaches the posterior capsular bag. Another useful example may be the monitoring of the OVD protection layer thickness to warn the surgeon of potential damage to the corneal endothelium.[32] The full eye volume capture scans shown in this work cover large FOVs and can be rendered and displayed intraoperatively after only few seconds of processing time. Such scans can be used to check the orientation and position of the IOL (e.g., centration) and tilt in the capsular bag intraoperatively, which may be important for the surgical outcome. They could also be utilized for reviewing and documenting corneal wound architecture at the end of surgery to prevent wound leakage

and ultimately reduce the risk for endophthalmitis. But given their vast imaging depth, these scans may also be used for intraoperative biometry. This could be particularly beneficial for patients with very dense cataracts or in trauma patients in whom optical preoperative measurements are not possible.

In conclusion, intraoperative SS-OCT provides significantly enhanced visualization capabilities such as larger scan depths for biometry measurements, faster raster capture scans for intraoperative use, and real-time imaging of the entire anterior chamber, allowing for IOL alignment determination, as compared to today's SD-OCT–based devices. Hence, if clinical studies can prove that certain uses impact patients' visual outcome, intraoperative OCT will very likely find its way into cataract surgery. Aside from its visualization capabilities, we anticipate cataract surgery to profit especially from advanced sensing capabilities generated from SS-OCT's spatial information and the valuable assistance functions that can be derived from it. Further into the future, intraoperative SS-OCT may play a critical role in robotic-assisted or even autonomous robotic cataract surgery.

Acknowledgments

The authors thank Carl Zeiss Meditec AG for funding and engineering support.

Supported by Carl Zeiss Meditec AG, Oberkochen, Germany.

Disclosure: **A. Britten**, (F); **P. Matten**, Carl Zeiss AG (E); **J. Nienhaus**, (F); **J.-M. Masch**, Carl Zeiss Meditec AG (E); **K. Dettelbacher**, (F); **H. Roodaki**, Carl Zeiss Meditec AG (E); **N. Hecker-Denschlag**, Carl Zeiss Meditec AG (E); **R.A. Leitgeb**, Carl Zeiss Meditec (C, F); **W. Drexler**, Carl Zeiss Meditec (C, F); **A. Pollreisz**, Bayer (C), Roche (C, F), Novartis (C), Oertli Instruments (C); **T. Schmoll**, Carl Zeiss Meditec (E)

References

1. Carrasco-Zevallos OM, Viehland C, Keller B, et al. Review of intraoperative optical coherence tomography: technology and applications [Invited]. *Biomedical Optics Express*. 2017;8(3):1607–1637.
2. Han SB, Liu YC, Mohamed-Noriega K, Mehta JS. Application of intraoperative optical coherence tomography technology in anterior segment surgery. *J Ophthalmol*. 2022;2022:1568406.
3. Nguyen P, Chopra V. Applications of optical coherence tomography in cataract surgery. *Curr Opin Ophthalmol*. 2013;24(1):47–52.
4. Creese K, Ong D, Zamir E. Should macular optical coherence tomography be part of routine preoperative cataract assessment? *Clin Exp Ophthalmol*. 2012;40(1):e118–e129.
5. Schallhorn JM, Tang M, Li Y, Song JC, Huang D. Optical coherence tomography of clear corneal incisions for cataract surgery. *J Cataract Refract Surg*. 2008;34(9):1561–1565.
6. Kumar DA, Agarwal A, Prakash G, Jacob S, Saravanan Y, Agarwal A. Evaluation of intraocular lens tilt with anterior segment optical coherence tomography. *Am J Ophthalmol*. 2011;151(3):406–412.e2.
7. Kim SJ, Equi R, Bressler NM. Analysis of macular edema after cataract surgery in patients with diabetes using optical coherence tomography. *Ophthalmology*. 2007;114(5):881–889.
8. Ehlers JP. Intraoperative optical coherence tomography: past, present, and future. *Eye (Lond)*. 2016;30(2):193–201.
9. Muijzer MB, Delbeke H, Dickman MM, et al. Outcomes of the advanced visualization in corneal surgery evaluation trial; a non-inferiority randomized control trial to evaluate the use of intraoperative OCT during Descemet membrane endothelial keratoplasty. *Front Ophthalmol*. 2023;2.
10. Zheng F, Deng X, Zhang Q, et al. Advances in swept-source optical coherence tomography and optical coherence tomography angiography. *Adv Ophthalmol Pract Res*. 2022;3:67–79.
11. Pasricha ND, Bhullar PK, Shieh C, et al. Four-dimensional microscope-integrated optical coherence tomography to visualize suture depth in strabismus surgery. *J Pediatr Ophthalmol Strabismus*. 2017;54:e1–e5.
12. Grewal DS, Bhullar PK, Pasricha ND, et al. Intraoperative 4-dimensional microscope-integrated optical coherence tomography-guided 27-gauge transvitreal choroidal biopsy for choroidal melanoma. *Retina*. 2017;37(4):796–799.
13. Pasricha ND, Shieh C, Carrasco-Zevallos OM, et al. Needle depth and big-bubble success in deep anterior lamellar keratoplasty: an ex vivo microscope-integrated OCT study. *Cornea*. 2016;35(11):1471–1477.
14. Pasricha ND, Shieh C, Carrasco-Zevallos OM, et al. Real-time microscope-integrated OCT to improve visualization in DSAEK for advanced bullous keratopathy. *Cornea*. 2015;34(12):1606–1610.
15. Hienert J, Amir-Asgari S, Matz H, Hirnschall N, Findl O. Evaluation of intraoperative aphakic

eye axial length measurements using swept-source OCT. *J Cataract Refract Surg*. 2022;48(6):663–666.
16. Ianchulev T, Hoffer KJ, Yoo SH, et al. Intraoperative refractive biometry for predicting intraocular lens power calculation after prior myopic refractive surgery. *Ophthalmology*. 2014;121(1):56–60.
17. Amir-Asgari S, Hirnschall N, Findl O. Using continuous intraoperative optical coherence tomography to classify swirling lens fragments during cataract surgery and to predict their impact on corneal endothelial cell damage. *J Cataract Refract Surg*. 2016;42(7):1029–1036.
18. Lytvynchuk LM, Glittenberg CG, Falkner-Radler CI, et al. Evaluation of intraocular lens position during phacoemulsification using intraoperative spectral-domain optical coherence tomography. *J Cataract Refract Surg*. 2016;42(5):694–702.
19. Li JD, Viehland C, Dhalla AH, et al. Visualization of surgical maneuvers using intraoperative real-time volumetric optical coherence tomography. *Biomed Opt Express*. 2023;14(7):3788–3811.
20. Grewal DS, Schultz T, Basti S, Dick HB. Femtosecond laser-assisted cataract surgery–current status and future directions. *Surv Ophthalmol*. 2016;61(2):103–131.
21. Carrasco-Zevallos OM, Keller B, Viehland C, et al. Live volumetric (4D) visualization and guidance of in vivo human ophthalmic surgery with intraoperative optical coherence tomography. *Sci Rep*. 2016;6:31689.
22. Britten A, Matten P, Weiss J, et al. Surgical microscope integrated MHz SS-OCT with live volumetric visualization. *Biomed Opt Express*. 2023;14(2):846–865.
23. Ginner L, Blatter C, Fechtig D, Schmoll T, Gröschl M, Leitgeb RA. Wide-field OCT angiography at 400 KHz utilizing spectral splitting. *Photonics*. 2014;1(4):369–379.
24. Langner S, Martin H, Terwee T, et al. 7.1 T MRI to assess the anterior segment of the eye. *Invest Ophthalmol Vis Sci*. 2010;51(12):6575–6581.
25. Nienhaus J, Britten A, Matten P, et al. Denoising of surgical microscope-integrated optical coherence tomography images. *Invest Ophthalmol Vis Sci*. 2023;64(8):2493–2493.
26. Weiss J, Sommersperger M, Nasseri A, Eslami A, Eck U, Navab N. Layer-aware iOCT volume rendering for retinal surgery. In: Lawonn K, Raidou RG, eds. *Eurographics Workshop on Visual Computing for Biomedicine*. Eurographics Proceedings; 2019.
27. Trout RM, Viehland C, Li J, et al. Feature-guided image fusion of intrasurgical optical coherence tomography and digital surgical microscopy. *Invest Ophthalmol Vis Sci*. 2021;62(11):16–16.
28. Bourcier T, Chammas J, Becmeur PH, et al. Robot-assisted simulated cataract surgery. *J Cataract Refract Surg*. 2017;43(4):552–557.
29. Chen CW, Francone AA, Gerber MJ, et al. Semiautomated optical coherence tomography-guided robotic surgery for porcine lens removal. *J Cataract Refract Surg*. 2019;45(11):1665–1669.
30. Draelos M, Tang G, Keller B, Kuo A, Hauser K, Izatt JA. Optical coherence tomography guided robotic needle insertion for deep anterior lamellar keratoplasty. *IEEE Trans Biomed Eng*. 2020;67(7):2073–2083.
31. Keller B, Draelos M, Zhou K, et al. Optical coherence tomography-guided robotic ophthalmic microsurgery via reinforcement learning from demonstration. *IEEE Trans Robot*. 2020;36(4):1207–1218.
32. Wust M, Matten P, Nenning M, Findl O. Thickness of the protective layers of different ophthalmic viscosurgical devices during lens surgery in a porcine model. *Transl Vis Sci Technol*. 2022;11(2):28.

Supplementary Material

Supplementary Video S1. Corneal incision in 4D.
Supplementary Video S2. OVD injection in 4D.
Supplementary Video S3. Capsulorrhexis in 4D.
Supplementary Video S4. Live B-scan of phacoemulsification.
Supplementary Video S5. Live B-scan of IOL unfolding.
Supplementary Video S6. Rendering of IOL position in capsular bag.